Boundary-Layer Meteorology Research Note manuscript No.
(will be inserted by the editor)

On the solution of katabatic flows with spatially varying eddy viscosity and diffusivity

M. G. Giometto · R. Grandi · J. Fang · M. B. Parlange

Received: DD Month YEAR / Accepted: DD Month YEAR

Abstract The Nieuwstadt closed form solution for the stationary Ekman layer is generalized for katabatic flows within the conceptual framework of the Prandtl model. The solution is valid for spatially-varying eddy viscosity and diffusivity (O'Brien type) and constant Prandtl number (Pr). Momentum and buoyancy transfer coefficients are specified in accordance with Monin-Obukhov similarity. The characteristics of the solution are discussed as a function of the dimensionless model parameters Pr and $\hat{z}_0\hat{N}^2\hat{b}_s^{-1}$, where $\hat{z}_0$ is the hydrodynamic roughness length, $\hat{b}_s$ is the imposed surface buoyancy and $\hat{N}$ is the Brunt-Väisälä frequency. For the considered range of such parameters, velocity and buoyancy profiles show significant variations in both phase and amplitude of extrema with respect to the classic constant K model and a more recent approximate solution based on the Wentzel-Kramers-Brillouin theory. Near-wall regions are characterized by relatively stronger surface momentum and buoyancy gradients, whose magnitude is inversely proportional to Pr. In addition, slope-parallel momentum and buoyancy fluxes are reduced, the low-level jet is further displaced toward the wall, and its peak velocity strongly depends on $\hat{z}_0\hat{N}^2\hat{b}_s^{-1}$.

M. G. Giometto
School of Architecture, Civil and Environmental Engineering, École Polytechnique Fédérale de Lausanne, Lausanne, Switzerland
E-mail: marco.giometto@epfl.ch

R. Grandi
Mathematics Institute for Geometry and Applications, École Polytechnique Fédérale de Lausanne, Lausanne, Switzerland

J. Fang
School of Architecture, Civil and Environmental Engineering, École Polytechnique Fédérale de Lausanne, Lausanne, Switzerland

M. B. Parlange
Dept. of Civil Engineering, Faculty of Applied Science, University of British Columbia, Vancouver, BC, Canada

1 Introduction

Slope winds are ubiquitous in nature and engineering, and they are of interest not only as a fundamental problem in itself, but also because of the important role they play over a broad range of scales and applications. On a local scale, for instance, they regulate local weather conditions, influencing atmospheric transport of momentum and scalars such as heat and humidity (Whiteman, 1990, 2000; Monti et al., 2002; Nylen et al., 2004; Rotach and Zardi, 2007; Lehner et al., 2015). On a regional scale, they can be responsible for intense cyclonic vorticity in the middle and upper troposphere (Parish and Bromwich, 1991; Parish, 1992; Parish and Bromwich, 1998). Persistent katabatic winds characterize the atmospheric boundary layer over Antarctica (Chu, 1987; Renfrew, 2004; Renfrew, I. and Anderson, P., 2006) and over glaciers (Oerlemans and Vugts, 1993; Oerlemans, 1994; Greuell et al., 1994, 1997; Smeets et al., 1997; Oerlemans, 1998; Oerlemans et al., 1999; Smeets et al., 2000; Oerlemans and Grisogono, 2002). Therefore an accurate characterization of such flows is an essential component of understanding and modeling of the weather and climate. The problematic geometrical setup complicates measurements (Oldroyd et al., 2016), whereas the complex dynamics (e.g. turbulent intermittency, waves, Kelvin-Helmholtz instabilities, low-level jets) and the lack of a satisfactory similarity theory for such flows (Nadeau et al., 2013) pose a challenge in terms of computational requirements for numerical modelers. In most cases the required resolution is in fact prohibitively costly (Fedorovich and Shapiro, 2009b,a; Burkholder et al., 2011). Because of this, conceptual models are still of great interest, and represent a valid tool for the characterization of such systems.

A cornerstone in the understanding of slope flows is represented by the classic Prandtl analytic model (Prandtl, 1942), afterwards extended to include Coriolis force (Gutman and Malbakhov, 1964), external winds (Lykosov and Gutman, 1972), and surface variability (Shapiro and Fedorovich, 2007; Oldroyd et al., 2014; Zardi and Serafin, 2015), to name but a few. The Prandtl model approximates the atmosphere in a Boussinesq sense and describes a steady stratified flow over a thermally perturbed unbounded planar sloping surface. It is summarized by the following system of ordinary differential equations:

$$-\hat{N}^2 \hat{u}(\hat{z}) \sin\alpha = [\hat{K}_H \hat{b}_{\hat{z}}]_{\hat{z}} \,, \tag{1a}$$

$$\hat{b}(\hat{z}) \sin\alpha = [\hat{K}_M \hat{u}_{\hat{z}}]_{\hat{z}} \,, \tag{1b}$$

where $\hat{(\cdot)}$ is used to denote a dimensional variable or parameter, $(\cdot)_{\hat{z}}$ denotes differentiation with respect to the slope-normal coordinate direction $\hat{z}$, $\hat{u}$ is the downslope velocity, $\hat{b} \equiv \hat{g}\hat{\theta}'/\hat{\theta}_0$ is buoyancy, where $\hat{g}$ is the gravitational acceleration, $\hat{\theta}'$ is the potential temperature perturbation (with respect to the background stably stratified environment characterized by the Brunt-Väisälä frequency $\hat{N}$), and $\hat{\theta}_0$ is a reference (constant) temperature; α is the slope angle and $\hat{K}_M$ and $\hat{K}_H$ denote the eddy viscosity and diffusivity (a model is used to parametrize turbulent fluxes of momentum and buoyancy, respectively). Equations are defined in $\hat{z} \in [\hat{z}_0, \infty)$ with boundary conditions $\hat{u}(\hat{z}_0) = 0$, $\hat{u}(\hat{z} \to \infty) = 0$, $\hat{b}(\hat{z}_0) = \hat{b}_s$ and $\hat{b}(\hat{z} \to \infty) = 0$ ($\hat{b}_s > 0$ for upslope flows, whereas $\hat{b}_s < 0$ for downslope flows). Eqs. 1 state that the slope-parallel component of buoyancy is balanced by momentum flux divergence, and that slope-parallel buoyancy advection is balanced by

buoyancy flux divergence. The flow is assumed to be invariant in the along-slope direction and the model can be used to determine the slope-normal ($\hat{z}$) structure of velocity $\hat{u}(\hat{z})$ and buoyancy $\hat{b}(\hat{z})$. The model is applicable far enough away from ridges and valleys that non-linear advection terms become small (Nappo and Shankar, 1987), and a balance between advection and diffusion (of both momentum and buoyancy) is achieved. This constraint is rather restrictive, as shown in Zardi and Serafin (2015). The Prandtl constant-K solution reads

$$\hat{b} = \hat{b}_s \exp\left(-\hat{\sigma}_c \hat{z}\right) \cos\left(\hat{\sigma}_c \hat{z}\right), \tag{2a}$$

$$\hat{u} = -\frac{\hat{b}_s}{NPr} \exp\left(-\hat{\sigma}_c \hat{z}\right) \sin\left(\hat{\sigma}_c \hat{z}\right), \tag{2b}$$

where

$$\hat{\sigma}_c^2 \equiv \frac{\hat{\sigma_0}}{2\hat{K_H}}, \qquad \text{and} \qquad \hat{\sigma}_0 \equiv \frac{\hat{N}\sin\left(\alpha\right)}{\sqrt{Pr}}. \tag{3}$$

The model is able to represent the low-level jet (LLJ) and the return flow region, key features of observed katabatic and anabatic flows. However, the constant-K solution is also known to be over-dissipative in the near-surface regions, and under dissipative above the LLJ regions (Defant, 1949; Oerlemans, 1998; Grisogono and Oerlemans, 2001). It is therefore not able to represent the observed strong surface gradients of temperature and momentum, and, in addition, the predicted wind speed typically decreases too rapidly away from the surface. Simple variations in the eddy diffusivity profiles were introduced in a patched analytic solution by Gutman (1983), whereas more recently Grisogono and Oerlemans (2001) considered general variations in the vertical structure of the eddy diffusivities, and derived a patched global solution based on the WKB approximation (Bender and Orszag, 1979). The WKB solution to the Prandtl equations, valid to leading-order in the inner layer and to first-order in the outer layer, reads

$$\hat{f}_{in} \sim \exp\left(-(1 \pm i)(\hat{\sigma}_0/2)^{1/2} \int_0^{\hat{z}} \hat{K}_H(z)^{-1/2} \mathrm{d}z\right) \qquad \hat{z} \in [\hat{z}_0, \hat{h}], \tag{4a}$$

$$\hat{f}_{out} \sim [\hat{K}_H(\hat{z})/\hat{K}_H(\hat{h})]^{-1/4} \exp\left(-(1 \pm i)(\hat{\sigma}_0/2)^{1/2} \int_0^{\hat{z}} \hat{K}_H(z)^{-1/2} \mathrm{d}z\right) \quad \hat{z} \in [\hat{h}, \infty), \tag{4b}$$

where $\hat{f}_{in} \equiv \hat{b}_{in} + i\hat{u}_{in}$ represents the inner-layer solution, and $\hat{f}_{out} \equiv \hat{b}_{out} + i\hat{u}_{out}$ is the outer-layer solution. $\hat{f}_{in}$ and $\hat{f}_{out}$ are patched at $\hat{z} = \hat{h}$, which separates the inner from the outer layer. The WKB solution is able to account for additional dynamics while still retaining an elegant form. However, WKB theory is only applicable when the model parameters ($\hat{K}_M, \hat{K}_H$) vary more slowly than the solution ($\hat{u}, \hat{b}$), and the validity of such a constraint for slope flows has been the subject of debate (Grisogono and Oerlemans, 2002).

Here, a closed-form solution to the Prandtl-model equations is derived on a finite domain ($\hat{z} \in [\hat{z}_0, \hat{H}]$), valid for eddy viscosity and diffusivity coefficients that are modeled as a limited range of cubic polynomials, similar to what was proposed in O'Brien (1970) for the planetary boundary layer. The derivation is a generalization of the solution proposed in Nieuwstadt (1983), where the Ekman-layer

equations were solved for the same form of momentum transfer coefficient. Recall that the Ekman-layer equations can be reduced to the Prandtl equations after simple changes of variables (Veronis, 1970). The solution, expressed as a combination of Gaussian hypergeometric functions, represents an exact alternative to the WKB formulation for the chosen form of the eddy diffusivities. Its sensitivity to variations in the parameter space are investigated here within the Monin-Obukhov framework, to provide insight on the coupling between the velocity and buoyancy fields.

2 Specification of $\hat{K}(\hat{z})$

Here, eddy diffusivities are prescribed in line with the classic O'Brien's model (O'Brien, 1970), viz.

$$\hat{K}(\hat{z}) = \kappa \hat{u}_* \hat{z}(1 - \hat{z}/\hat{H})^2 \qquad \hat{z} \in [\hat{z}_0, \hat{H}]\,, \tag{5}$$

where κ is the von Kármán constant, $\hat{u}_* = \kappa(\hat{z}\hat{u}_{\hat{z}})|_{\hat{z}_0}$ is the friction-velocity, and $\hat{H}$ is the height of the domain, controlling both shape and magnitude of $\hat{K}$. The O'Brien model complies with the $\hat{K}$-requirements defined in Grisogono and Oerlemans (2002), and has often been used in studies of stable boundary layers (see for instance Pielke (1984) and Stull (1988)). A generalized O'Brien model was also recently adopted in Grisogono and Oerlemans (2001) to study katabatic flows. In the original O'Brien's formulation $\hat{H}$ corresponds to the boundary layer depth; in this study $\hat{H} = 3\hat{h}$ is evaluated iteratively under the constraint $\hat{h} = \hat{z}_r$, where $\hat{z}_r$ is the height of the peak velocity magnitude in the return flow region. Such a choice for $\hat{h}$ is based on a sensitivity analysis that was performed using direct numerical simulations to resolve katabatic flows over steep slopes ($\alpha \geq 15^\circ$).

Given the current lack of a rigorous similarity theory for katabatic flows, this study is restricted to the Monin-Obukhov framework, which is expected to yield acceptable approximations of transfer coefficients in the near-surface regions (Gutman, 1983). Monin-Obukhov similarity is not expected to hold in the above-jet regions, where eddy viscosity and diffusivity coefficients are likely to depend on an additional set of parameters such as the sloping angle (α), the Brunt-Väisälä frequency ($\hat{N}$), and the imposed surface buoyancy $\hat{b}_s$ (or buoyancy flux). Nevertheless, the proposed solution is valid in a more general sense, and could easily be adapted in the future to a different $\hat{K}$-parameterisation. For instance, one could easily choose a different prefactor than κ, to make it depend on the model parameters. Knowledge of $\hat{u}_*$ and $\hat{H}$ (or equivalently $\hat{h}$) allows one to specify $\hat{K}(\hat{z}) = \kappa \hat{u}_* \hat{z}(1 - \hat{z}/\hat{H})^2$.

3 The Analytic Solution

For the combination

$$\hat{f} = \hat{b} - (i\hat{N}\sqrt{Pr})\hat{u} \tag{6}$$

the system of Eqs. 1 is reduced to a complex ordinary differential equation (ODE) for the canonical variable $\hat{f}$:

$$\hat{f} = \left[\frac{-i\hat{K}_M(\hat{z})}{\hat{N}\sin(\alpha)\sqrt{Pr}} \hat{f}_{\hat{z}} \right]_{\hat{z}} \qquad \hat{z} \in [\hat{z}_0, \hat{H}]\,, \tag{7}$$

with boundary conditions $\hat{f}(\hat{z}_0) = \hat{b_s}$ and $\hat{f}(\hat{H}) = 0$. Assigning a length, velocity and buoyancy scale $\hat{L} = \hat{u}_*\kappa(\hat{N}\sin\alpha)^{-1}$, $\hat{U} = |\hat{b}_s|\hat{N}^{-1}$ and $\hat{B} = |\hat{b}_s|$ respectively, Eq. 7 reduces to:

$$f = \frac{-i}{\sqrt{Pr}}\left[K_M(z)f_z\right]_z \qquad z \in [z_0, H]\,, \tag{8}$$

where $K_M(z) = z(1 - z/H)^2$ is the normalised eddy viscosity, $z = \hat{z}\hat{L}^{-1}$, $f = \hat{b}\hat{B}^{-1} + (i\sqrt{Pr})\hat{u}\hat{U}^{-1}$, $H = \hat{H}\hat{L}^{-1}$ and $z_0 = \hat{z_0}\hat{L}^{-1}$, with boundary conditions $f(z_0) = -1$, $f(H) = 0$. The canonical form of Eq. 8 reads:

$$f_{zz} + Pf_z + Qf = 0, \tag{9}$$

where $P(z) = K_{M,z}/K_M$ and $Q(z) = (-i\sqrt{Pr})/K_M$. Second, it is straightforward to show that rewriting Eq. 9 for $y = \frac{z}{H}$ results in

$$f_{yy} + \widetilde{P}f_y + \widetilde{Q}f = 0, \tag{10}$$

where $\widetilde{P}(y) = \gamma_y(y)/\gamma(y)$ and $\widetilde{Q}(y) = (-i\sqrt{Pr}H)/\gamma(y)$, with $\gamma(y) = y(y-1)^2$. Eq. 10 is a second order ordinary differential equation with three regular singular points at $y = 0, 1$ and ∞, as in Morse and Feshbach (1953). This specific equation is known as the *equation of Papperitz* and its general solution is:

$$f(y) = \alpha(1-y)^{\mu}\,{}_2F_1(\mu, 1-\mu', 1+\mu-\mu', 1-y)+\beta(1-y)^{\mu'}\,{}_2F_1(\mu', 1-\mu, 1+\mu'-\mu, 1-y)\,, \tag{11}$$

where ${}_2F_1$ are *Gaussian hypergeometric functions* and μ, μ' are the solutions to the quadratic equation

$$x^2 + x - iH\sqrt{Pr} = 0.$$

Upon back-substitution of the independent variable and specification of the integration constants α and β (through the imposition of boundary conditions), the solution in terms of u and b is derived by separating the real and imaginary part of f

$$u(z) = -\frac{\mathrm{Im}(f(z))}{\sqrt{Pr}}, \qquad b(z) = \mathrm{Re}(f(z)). \tag{12}$$

As stated in the introduction, the proposed derivation closely resembles that in Nieuwstadt (1983), where the Ekman-layer equations have been solved in closed form for the same eddy viscosity coefficient. Here, the solution is specified for the Prandtl model equations, and generalised to account for arbitrary (constant) Pr. In addition, the proposed solution considers a finite z_0, as opposite to that in Nieuwstadt (1983) where the simplifying assumption $z_0 = 0$ was adopted. A finite z_0 (hence finite $K_M(z_0)$ and $K_H(z_0)$) is required when solving the Prandtl slope flow model, which would otherwise yield unphysical velocity and buoyancy profiles. The formulation of $K_M(z)$ and $K_H(z)$ allows for exact integration of Eqs. 1, hence providing a reference to study the dependence of the flow on the dimensionless model parameters Pr and $z_0 \equiv \hat{z}_0\hat{u}_*\kappa(\hat{N}\sin\alpha)^{-1}$. It also represents a useful reference for the validation of numerical and patched/matched solutions.

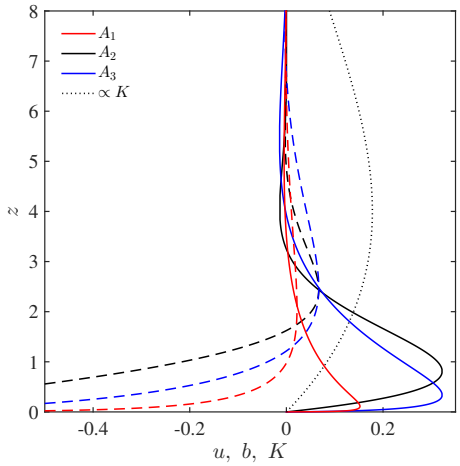

Fig. 1 Comparison of the proposed analytic solution (A1) against the constant-K (A2) and the WKB solution (A3). u is positive in the down-slope direction. The dashed black line identifies the adopted eddy viscosity K_M. The constant-K value is fixed to $K_M^{\mathrm{A2}} = \max(K_M^{\mathrm{A1}})/3$. Velocity profiles ($u$) are denoted with solid lines whereas buoyancy profiles (b) are denoted by dashed lines. Here $z_0 = 0.001$, $Pr = 1$ and $H = 12$. Assuming $\hat{N} = 10^{-2}$ (Hz), $\hat{\alpha} = 5°$ and $\hat{b}_s = -0.1$ (m s^{-2}), the corresponding dimensional system, based on $u_* \equiv \hat{u}_* U^{-1}$ from the A1 solution, is characterized by $\hat{z}_0 = 0.08$ (m) and $\hat{u}_* = 0.18$ (m s^{-1}), within the range of commonly observed atmospheric values. A1 is indistinguishable to a corresponding second-order centered finite-difference numerical solution (also exact in double precision arithmetics), therefore the comparison is omitted.

4 Examples

In Fig. 1 we compare the proposed analytic solution (A1) against the constant-K (A2) and the WKB solution (A3), considering $Pr = 1$ (i.e., $\hat{K}_M = \hat{K}_H$). The constant-K solution is evaluated based on Eqs. 2, and the WKB solution is evaluated based on Eqs. 4. For the sake of comparison, A1 and A3 are evaluated for the same z_0 and H (hence same $K(z)$) parameters, whereas A2 is computed imposing $K_{A2} = \max(K)/3$. $\hat{h}$ is evaluated iteratively in order to match z_r of the A1 solution. Given that the resulting A1 solution is relatively insensitive to the exact $\hat{h}$ (in the neighborhood of the $\hat{h} = \hat{z}_r$ value) only a few iterations are necessary to provide a good approximation of the desired $\hat{K}$. The chosen $K(z)$ satisfies the constraints defined in Grisogono and Oerlemans (2002) for the validity of the WKB method. A1 shows a remarkably strong inversion in the near surface regions, when compared against its analytical counterparts, suggesting an over-diffusive behavior of both A2 and A3. For instance, normalised surface buoyancy gradients of simulation A1 are over an order of magnitude larger than those of A3 ($b_z^{\mathrm{A1}}/b_z^{\mathrm{A3}} = \mathcal{O}(10)$ for $z \to z_0$). Nevertheless, $u_z^{\mathrm{A1}} \approx u_z^{\mathrm{A3}}$ for $z \to z_0$, confirming the better dissipative properties of A3, when compared against the constant-K approach. To underline the importance of a decreasing magnitude of eddy diffusivities as the surface is approached, it is worth noting that $u_z^{\mathrm{A1}}/u_z^{\mathrm{A2}} = \mathcal{O}(10)$. Overall, the proposed normalised solution differs significantly when compared against A2 and A3, in both

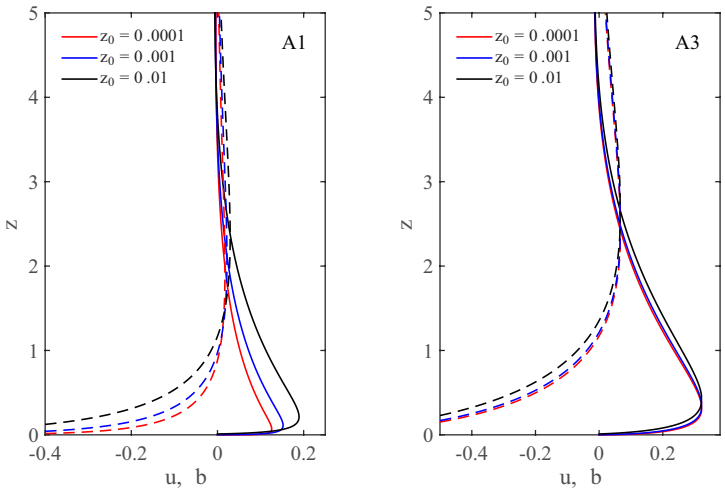

Fig. 2 Sensitivity of the normalised A1 (left) and A3 (right) solutions to the z_0 parameter. Solid lines denote down-slope velocity (u) whereas dashed lines denote buoyancy (b). Fixed parameters: $H = 12$, $Pr = 1$.

amplitude and location of extrema. Both the height of the LLJ and the peak velocity are significantly reduced, features that are of great importance for an accurate representation of the stable boundary layer and from a parameterisation perspective (Mahrt, 1998). Besides, A1 predicts significantly reduced mass and buoyancy (slope-parallel) fluxes, viz. $\int_0^H u\,\mathrm{d}z$ and $\int_0^H b\,\mathrm{d}z$, with respect to A2 and A3.

The sensitivity of the solution to variations in the z_0 parameter is displayed in Fig. 2. Since $(u_*, b_*) \propto z_0$, where $b_* \equiv \kappa z b_z$, larger hydrodynamic roughness lengths (z_0) correspond to stronger transfer rates of momentum and buoyancy in the vertical direction, yielding a larger z_j and $\max(u)$. To highlight differences with respect to the WKB solution, the same z_0 sensitivity test is displayed for the A3 solution in Fig. 2. Because $K \approx z$ in the neighborhood of $z = z_0$, A3 predicts $z_j \approx \pi^2/32 + z_0$ and $\max(u) = 0.32$. A3 is therefore able to describe the z_0 (alias K) dependency of z_j, but predicts a K-invariant $\max(u)$, as is clear from Fig. 2. A2 is also characterized by a K-invariant $\max(u)$. The proposed solution therefore provides additional insight on the physics of the system, valid within the underlying Monin-Obukhov framework and idealized boundary conditions, suggesting a somewhat different coupling between the velocity and buoyancy fields, when compared to that predicted by previous analytic solutions of the linear Prandtl model. It shows that a larger z_0 parameter results in a higher and stronger LLJ ($[z_j, \max(u)] \propto z_0$). Further, since $\hat{L} = \kappa \hat{u}_* / (\hat{N} \sin\alpha)$, the characteristic scale of the flow ($\hat{L}$) will vary proportionally to z_0 for a prescribed $\hat{U}, \hat{B}, \alpha$ set.

Under stably stratified environments, pressure fluctuations induced by breaking gravity waves sum to those induced by turbulence, and yield an increase in the total momentum flux, without directly influencing the buoyancy flux (Mahrt, 1998). This results in turbulent Prandtl numbers that are usually greater than unity. Variations by a factor of 2 for Pr, perhaps even more under conditions of strong

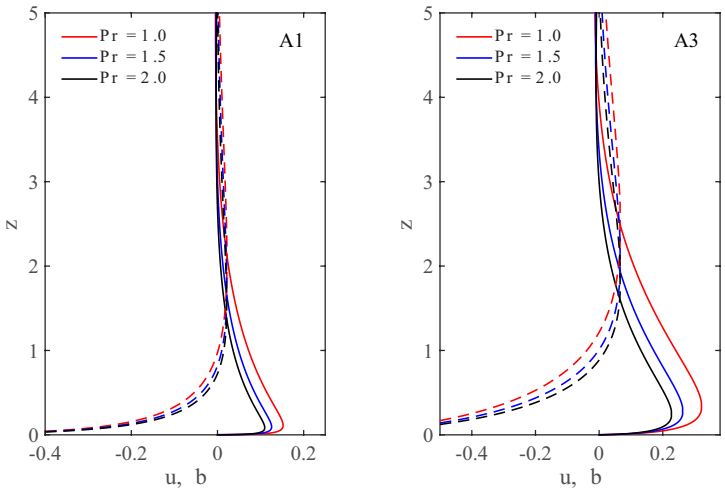

Fig. 3 Sensitivity of the normalised A1 (left) and A3 (right) solutions to the Pr parameter. Solid lines denote down-slope velocity (u) and dashed lines denote buoyancy (b). Displayed solutions correspond to: $H = 12$, $z_0 = 0.001$.

stratification, are common and that can lead to considerable changes in the shapes of vertical profiles of velocity and buoyancy. The sensitivity of the solution to variations in the Pr parameter is displayed in Fig. 3. As before in Fig. 2, the closed form solution (A1) is compared to the WKB solution (A3). Variations in Pr change the solution throughout the domain for both A1 and A3, larger Pr results in weaker thermal and dynamic boundary-layers, and in a proportional decrease in u_j and z_j. Such a behavior could have been anticipated, since a larger Pr in conjunction with the constant (imposed) surface buoyancy is expected to result in a lower surface buoyancy flux, i.e. in a lower rate of potential energy injected into the system.

To study the sensitivity of the solution on the h parameter we considered a $\pm 10\%$ h-variation, and results are displayed in Fig. 4. Despite the non-negligible changes in $K(z)$ in the outer regions of the flow we observe a modest $\approx \pm 0.5\%$ variation in $\max(u)$ and a $\approx \pm 5\%$ variation in z_j, $\min(u)$ and z_r (the location of $\min(u)$), which is well within the degree of accuracy of the current study. Recall that variations in h lead to the same first order Taylor expansion of $K(z)$ around z_0, therefore the inner regions of the flow are relatively insensitive to the exact h value.

5 On the computation of the solution

The computation of the Gauss hypergeometric function ${}_2F_1$ with all its parameters complex is known to be a non-trivial task. Although the ${}_2F_1$ function is merely a power series expansion (whose implementation is immediate), its use is prone to cancellation and round-off error, which become especially significant for certain

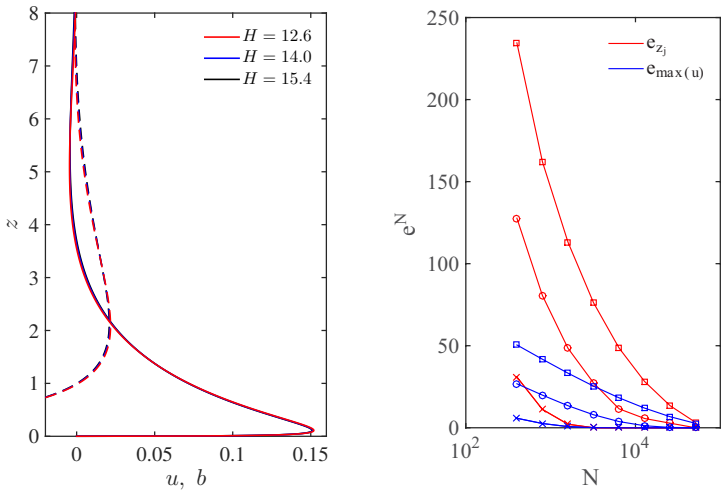

Fig. 4 Left plot: Sensitivity of velocity u (solid lines) and buoyancy b (dashed lines) profiles on the H parameter for the A1 solution. Right plot: convergence test, relative percentage error for z_j (red lines) and $\max(u)$ (blue lines) as a function of N, where N represents the number of terms considered in the truncated ${}_2F_1$ series. Parameters for the H-sensitivity study (left plot): $H_1 = 11.2$, $H_2 = 14$, $H_3 = 16.8$ and $z_0 = 0.001$. Parameters for the convergence test (right plot): $z_0 = 0.00001$ (squares), $z_0 = 0.0001$ (circles), $z_0 = 0.001$ (crosses) and $H = 14$. We define $e_{z_j} = 100(z_j^N - z_j)/z_j$ and $e_{\max(u)} = 100[\max(u^N) - \max(u)]/\max(u)$, where $(\cdot)^N$ represents a quantity computed truncating the ${}_2F_1$ series to N terms, and where z_j and $\max(u)$ represent quantities that are exact in double precision arithmetic.

ranges of the parameters and of the independent variable (Temme, 2007). In our case, the solution $f = b + iu$ is evaluated in $y \in (z_0/H, 1)$, which is within the radius of convergence (R) of the hypergeometric functions that define f (the radius of convergence of ${}_2F_1(a, b, c, y)$ is $|y| = 1$). The solution computed here represents the ${}_2F_1$ functions as truncated power series, i.e. ${}_2F_1(a, b, c, y) = [(a)_k(b)_k]/[(c)_k k!]y^k$, where a, b, c are the three input parameters, $(\cdot)_k$ is the Pochhammer symbol and $k!$ denotes the factorial of $k = 1, 2, \ldots N$. All computations are performed in double precision arithmetic. In Fig. 4 we display the convergence of the solution, in terms of z_j and $\max(u)$, for a given set of z_0 values and $H = 10$. The solution shows sub-logarithmic convergence for both $e_{z_j} = 100(z_j^N - z_j)/z_j$ and $e_{\max(u)} = 100[\max(u^N) - \max(u)]/\max(u)$, and clearly, the smaller the z_0 parameter, the slower the resulting convergence rate. This behavior is justified by the fact that as z_0 is reduced, the solution is evaluated closer to R, where the convergence of ${}_2F_1$ in its power series form is known to be retarded. Despite the slow convergence of the series summation, the evaluation of the solution is stable throughout the range of realistic z_0. Note that the efficacy of the series summation could be much improved by various techniques (e.g., Shanks method, Padé summation, etc.), but such an analysis is beyond the goal of the current study.

6 Conclusions

A closed form solution of the Prandtl model equations has been proposed herein, valid for O'Brien-type eddy diffusivities and constant Prandtl number. The solution is for katabatic flows and is an adaptation of the solution proposed in Nieuwstadt (1983) for the Ekman-layer equations, generalized to account for constant $Pr \neq 1$. Its characteristics have been discussed assuming transfer coefficients for momentum and buoyancy in accordance to Monin-Obukhov similarity (albeit the solution lend itself to more general K-parameterisations). The dependence of the normalised solution on the model dimensionless parameters Pr and $\hat{z}_0 \hat{N}^2 \hat{b}_s^{-1}$ has been tested and compared against corresponding WKB solutions. For the same geometrical and physical parameters, profiles show significant variations in both phase and amplitude of extrema with respect to their WKB counterparts: stronger surface gradients (inversely proportional to Pr) are combined with overall reduced slope-parallel fluxes, and the LLJ is further displaced toward the wall. In addition, its peak velocity, LLJ height, and surface gradients proved to be highly sensitive to variations of the dimensionless parameter $\hat{z}_0 \hat{N}^2 \hat{b}_s^{-1}$, highlighting a more complex coupling between the velocity and buoyancy fields. Despite the slow convergence of the series summation, which can however be accelerated through various techniques, the evaluation of the solution is stable throughout the range of realistic z_0. The proposed model can be of use to validate numerical or patched / matched solutions of the Prandtl equations, and to improve future stable boundary layer parameterisations, when coupled with other parts of the boundary layer physics.

7 Acknowledgements

This research was funded by the Swiss National Science Foundation (SNSF-200021-134892), the Competence Center for Environmental Sustainability (CCES-SwissEx) of the ETH domain, and the NSERC Discovery Grant program. We are grateful to the peer reviewers whose comments helped to improve the overall quality of the manuscript.

References

Bender CM, Orszag SA (1979) Advanced mathematical methods for scientists and engineers, vol 63

Burkholder B, Fedorovich E, Shapiro A (2011) Evaluating subgrid-scale models for large-eddy simulation of turbulent katabatic flow. In: Quality and reliability of large-eddy simulations II, Springer Netherlands, Dordrecht, ERCOFTAC Series, pp 149–160

Chu PC (1987) An instability theory of ice-air interaction for the formation of ice edge bands. J Geophys Res 92(C7):6966–6970

Defant F (1949) Zur theorie der hangwinde, nebst bemerkungen zur theorie der berg- und talwinde. Archiv für Meteorologie, Geophysik und Bioklimatologie Serie A 1:421–450

Fedorovich E, Shapiro A (2009a) Structure of numerically simulated katabatic and anabatic flows along steep slopes. Acta Geophys 57(4):981–1010

Fedorovich E, Shapiro A (2009b) Turbulent natural convection along a vertical plate immersed in a stably stratified fluid. J Fluid Mech 636:41–57
Greuell JW, Broeke Van den MR, Knap W, Reijmer C, Smeets P, , Struijk I (1994) PASTEX: A glacio-meteorological experiment on the Pasterze (Austria). Tech. rep., Institute forMarine and Atmospheric Research, Utrecht University, Utrecht
Greuell W, Knap WH, Smeets PC (1997) Elevational changes in meteorological variables along a midlatitude glacier during summer. J Geophys Res 102(25):941–954
Grisogono B, Oerlemans J (2001) Katabatic flow: Analytic solution for gradually varying eddy diffusivities. J Atmos Sci 58(21):3349–3354
Grisogono B, Oerlemans J (2002) Justifying the WKB approximation in pure katabatic flows. Tellus 54(5):453–462
Gutman LN (1983) On the theory of the katabatic slope wind. Tellus 35A:213–218
Gutman LN, Malbakhov VM (1964) On the theory of the katabatic winds of Antarctica. Met Issled 9:150–155
Lehner M, Whiteman CD, Hoch SW, Jensen D, Pardyjak ER, Leo LS, Di Sabatino S, Fernando HJS (2015) A case study of the nocturnal boundary layer evolution on a slope at the foot of a desert mountain. J Appl Meteorol Clim 54(4):732–751
Lykosov VN, Gutman LN (1972) Turbulent boundary layer above a sloping underlying surface. Proc USSR Acad Sci 8:799–809
Mahrt L (1998) Stratified atmospheric boundary layers and breakdown of models. Theor Comput Fluid Mech 11:263–279
Monti P, Fernando HJS, Princevac M, Chan WC, Kowalewski TA, Pardyjak ER (2002) Observations of flow and turbulence in the nocturnal boundary layer over a slope. J Atmos Sci 59(17):2513–2534
Morse PM, Feshbach H (1953) Methods of theoretical physics. McGraw-Hill
Nadeau DF, Pardyjak ER, Higgins CW, Parlange MB (2013) Similarity scaling over a steep alpine slope. Boundary-Layer Meteorol 147(3):401–419
Nappo CJ, Shankar RK (1987) A model study of pure katabatic flows. Tellus 39(1):61–71
Nieuwstadt FTM (1983) On the solution of the stationary, baroclinic Ekman-layer equations with a finite boundary-layer height. Boundary-Layer Meteorol 26(4):377–390
Nylen TH, Fountain AG, Doran PT (2004) Climatology of katabatic winds in the McMurdo dry valleys, southern Victoria Land, Antarctica. Journal of Geophysical Research: Atmospheres 109(D3):1–9
O'Brien JJ (1970) A note on the vertical structure of the eddy exchange coefficient in the planetary boundary layer. J Atmos Sci 27(8):1213–1215
Oerlemans J (1994) Quantifying global warming from the retreat of glaciers. Science 264(5156):243–245
Oerlemans J (1998) The atmospheric boundary layer over melting glaciers. In: Clear and Cloudy Boundary Layers, Royal Netherlands Academy of Arts and Sciences, pp 129–153
Oerlemans J, Grisogono B (2002) Glacier winds and parameterisation of the related surface heat fluxes. Tellus 54(5):440–452
Oerlemans J, Vugts HF (1993) A meteorological experiment in the melting zone of the Greenland ice sheet. Bull Am Meteorol Soc 74(3):355–365

359 Oerlemans J, Björnsson H, Kuhn M, Obleitner F, Palsson F, Smeets CJPP, Vugts
360 HF, Wolde JD (1999) Glacio-meteorological investigation on Vatnajokull, Ice-
361 land, summer 1996: An overview. Boundary-Layer Meteorol 92(1):3–24
362 Oldroyd HJ, Katul GG, Pardyjak ER, Parlange MB (2014) Momentum balance of
363 katabatic flow on steep slopes covered with short vegetation. Geophys Res Lett
364 41(13):4761–4768
365 Oldroyd HJ, Pardyjak ER, Huwald H, Parlange MB (2016) Adapting tilt cor-
366 rections and the governing flow equations for steep, fully three-dimensional,
367 mountainous terrain. Boundary-Layer Meteorology, In Press
368 Parish TR (1992) On the role of Antarctic katabatic winds in forcing large-scale
369 tropospheric motions. J Atmos Sci 49(15):1374–1385
370 Parish TR, Bromwich DH (1991) Continental-scale simulation of the Antarctic
371 katabatic wind regime. J Clim 4(2):135–146
372 Parish TR, Bromwich DH (1998) A case study of Antarctic katabatic wind inter-
373 action with large-scale forcing. Mon Weather Rev 126(1):199–209
374 Pielke RA (1984) Mesoscale numerical modeling. Adv Geophys 23:185–344
375 Prandtl L (1942) Führer durch die strömungslehre. Vieweg & Sohn, Braunschweig
376 Renfrew IA (2004) The dynamics of idealized katabatic flow over a moderate slope
377 and ice shelf. Q J R Meteorol Soc 130(598):1023–1045
378 Renfrew, I A, Anderson, P S (2006) Profiles of katabatic flow in summer and
379 winter over Coats Land, Antarctica. Q J R Meteorol Soc 132(616):779–802
380 Rotach MW, Zardi D (2007) On the boundary-layer structure over highly complex
381 terrain: Key findings from MAP. Q J R Meteorol Soc 133(625):937–948
382 Shapiro A, Fedorovich E (2007) Katabatic flow along a differentially cooled sloping
383 surface. J Fluid Mech 571:149–175
384 Smeets CJPP, Duynkerke PG, Vugts HF (1997) Turbulence characteristics of the
385 stable boundary layer over a mid-latitude glacier. part 1: a combination of kata-
386 batic and large-scale forcing. Boundary-Layer Meteorol 87:117–145
387 Smeets CJPP, Duynkerke PG, Vugts HF (2000) Turbulence characteristics of the
388 stable boundary layer over a mid-latitude glacier. Part 2: pure katabatic forcing
389 conditions. Boundary-Layer Meteorol 97:73–107
390 Stull RB (1988) An introduction to boundary layer meteorology. Kluwer Academic
391 Publishers, Dordrecht
392 Temme NM (2007) Numerical aspects of special functions. Acta Numer 16:379–478
393 Veronis G (1970) The analogy between rotating and stratified fluids. Annu Rev
394 Fluid Mech 2(1):37–66
395 Whiteman CD (1990) Observations of thermally developed wind systems in moun-
396 tainous terrain. Atmos Process over complex terrain, Meteor Monogr 45:5–42
397 Whiteman CD (2000) Mountain meteorology: Fundamentals and applications.
398 Mountain Research and Development 21(1):355
399 Zardi D, Serafin S (2015) An analytic solution for time-periodic thermally driven
400 slope flows. Q J R Meteorol Soc 141(690):1968–1974